GERALDINE (Google earth Engine supRaglAciaL Debris INput dEtector) - A new Tool for Identifying and Monitoring Supraglacial Landslide Inputs

William D. Smith[1], Stuart A. Dunning[1], Stephen Brough[1,2], Neil Ross[1], Jon Telling[3]

[1] School of Geography, Politics and Sociology, Newcastle University, Newcastle upon Tyne, UK.
[2] Department of Geography and Planning, School of Environmental Sciences, University of Liverpool, UK.
[3] School of Natural and Environmental Sciences, Newcastle University, Newcastle upon Tyne, UK.

Correspondence to: William D. Smith (w.d.smith2@newcastle.ac.uk)

Abstract. Rock avalanches, a high-magnitude, long runout form of bedrock landslide, are thought to increase in frequency as a paraglacial response to ice-retreat/thinning, and arguably, due to warming temperatures/degrading permafrost above current glaciers. However, our ability to test these assumptions by quantifying the temporal sequencing of debris inputs over large spatial and temporal extents is limited in areas with glacier ice. Discrete landslide debris inputs, particularly in accumulation areas are rapidly 'lost', being reworked by motion and icefalls, and/or covered by snowfall. Although large landslides can be detected and located using their seismic signature, small to medium-sized landslides, particularly supraglacially deposited landslides which feature a "quiet" runout over snow, frequently go undetected because their seismic signature is less than the noise floor. Here, we present GERALDINE (Google earth Engine supRaglAciaL Debris INput dEtector): a new open-source tool leveraging Landsat 4-8 satellite imagery and Google Earth Engine. GERALDINE outputs maps of new supraglacial debris additions within user-defined areas and time ranges, providing a user with a reference map, from which large debris inputs such as supraglacial rock avalanches can be rapidly identified. We validate the effectiveness of GERALDINE outputs using published rock-avalanche inventories, then demonstrate its potential by identifying two previously unknown, large (>2 km2) supraglacial debris inputs onto glaciers in the Hayes Range, Alaska, one of which was not detected seismically. GERALDINE is a first step towards a revised global magnitude-frequency of rock avalanche inputs onto glaciers over the 37 years of Landsat Thematic Mapper imagery.

1.0 Introduction

There are currently 215,547 glaciers worldwide covering >700,000 km^2, excluding the Greenland and Antarctic ice sheets (RGI Consortium, 2017). Supraglacial debris covers 4.4% of this glacier area (Scherler et al., 2018) but for many glaciers it plays a critical role in controlling a glaciers response to climate change, due to its influence on surface ablation and mass loss (Benn et al., 2012; Mihalcea et al., 2008a, 2008b; Nicholson and Benn, 2006; Östrem, 1959; Reznichenko et al., 2010). Extensive debris coverage can alter the hydrological regime of a glacier (Fyffe et al., 2019), with the potential to

increase/decrease downstream freshwater availability (Akhtar et al., 2008), and can play a key role in controlling rates of glacier thinning and/or recession, subsequently contributing to sea level rise (Berthier et al., 2010). This supraglacial debris control is thought to be increasingly important with more negative glacier mass balances, with retreating glaciers being increasingly characterised by expanding debris cover extents (Scherler et al., 2011b; Tielidze et al., 2020). The expansion of

35 supraglacial debris cover is due to: (i) glaciological controls such as thrusting and meltout of sub- and en-glacial sediment onto the surface (e.g. Kirkbride & Deline, 2013; Mackay et al., 2014; Wirbel et al., 2018); and, (ii) debris input from surrounding valley walls through bedrock mass movements (Deline et al., 2014; Porter et al., 2010); and, (iii) remobilisation of debris stores, particularly lateral moraines (Van Woerkom et al., 2019). The relative contributions of 'glacially' derived sediment, which may in fact be the re-emergence of glacially modified mass movements (Mackay et al., 2014), as compared to direct

40 subaerial inputs, is highly variable and there is complex coupling between hillslopes and glaciers that varies with relief (Scherler et al., 2011a). However, recent evidence from the Greater Caucasus region (Eurasia) suggests that supraglacially deposited rock avalanches (RAs), attributed to processes associated with climate change, are a key factor in increasing supraglacial debris coverage (Tielidze et al. 2020). Here we focus on the inputs of RAs, high magnitude ($> 10^6$ m^3), perceived low frequency, long runout landslides where there is disparity between current high rates of activity above ice (Allen et al.,

45 2011; Coe et al., 2018) and our ideas of lagged paraglacial slope responses (Ballantyne, 2002; Ballantyne et al., 2014a).

Dating of deposits has shown that large RAs are thought to lag ice-free conditions by some thousands of years (Ballantyne et al., 2014b; Pánek et al., 2017). Events cluster in deep glacially eroded troughs and inner gorges relatively low in the landscape (Blöthe et al., 2015). Numerical modelling has shown how considerable rock-mass damage is possible during the first

50 deglaciation cycle (Grämiger et al., 2017); some of the largest inventories highlight a close association with former glacier limits and the source zones of RAs, particularly in the vicinity of glacial breaches (Jarman and Harrison, 2019). However, almost all of our knowledge of past events relies on the presence of in-situ RA deposits. Due to erosional and depositional censuring such deposits are heavily biased to ice-free landscapes where rates of unmodified preservation are higher, although these are still unlikely to constrain true magnitude-frequencies unless rates of geomorphic turn-over are low (Sanhueza-Pino

55 et al., 2011). In glaciated areas supraglacial landslide deposits are rapidly transported away from source areas, removing the simplest diagnostic evidence of a subaerial mass movement process – a linked cavity and debris deposit. Fresh snowfall or wind redistribution can rapidly cover a rock-avalanche deposit that is many kilometres square in area (Dunning et al., 2015). If this occurs within the accumulation zone the deposit is essentially lost to all surface investigation and non-penetrating remote sensing until eventual re-emergence in the ablation zone, after considerable modification by transport processes. If a RA is

60 emplaced into the ablation zone, censoring may be seasonal, but through time surface transport disrupts initially distinctive emplacement forms (Uhlmann et al., 2013). This supraglacial debris loading represents a glacier input (Jamieson et al., 2015) and can alter glacier mass balance, influence localised melt regimes (Hewitt, 2009; Reznichenko et al., 2011), and glacier velocity (Bhutiyani and Mahto, 2018; Shugar et al., 2012), leading to speed-ups and terminus positions asynchronous with current climatic conditions. Sometimes this leads to moraines that are out of phase with climate, due to the reduction in surface

65 ablation and surging (or the slowing of a retreat) caused by large landslide inputs (Hewitt, 1999; Reznichenko et al., 2011; Shulmeister et al., 2009; Tovar et al., 2008; Vacco et al., 2010).

Currently, the detection of large supraglacial debris inputs – other than through the most common form of ground-based detection, eye-witness reporting – is through the application of optical satellite imagery. This is a labour and previously
70 computationally intensive process, often involving the downloading, pre-processing and manual analysis of large volumes (gigabytes) of satellite imagery. In Alaska, Uhlmann et al. (2013) used ablation zone Landsat mosaics to suggest the frequency of supraglacial debris inputs from large landslides is underestimated, and increasing over time. Seismic monitoring can also be used to detect large debris inputs onto glacier surfaces (Ekström and Stark, 2013) utilising the global seismic network to detect long-period surface waves, characteristic of seismogenic landslides. Seismic methods have identified some of the largest
75 supraglacially deposited RAs in recent times (e.g. Lamplugh glacier RA (Dufresne et al., 2019)) which are compiled in a database (IRIS DMC, 2017), and, when combined with manual analysis of satellite imagery, gives information on duration, momenta, potential energy loss, mass and runout trajectory. However, landslides are challenging to detect using seismic methods and event positional accuracy is limited to a 20 – 100 km radius, due to the lack of high frequency waves when compared to earthquakes, further inhibited by the low frequencies and long wavelengths of dominant seismic waves worldwide
80 (Ekström and Stark, 2013). This also results in an inability to detect smaller landslides due to their weak seismic fingerprint (< 5.0 magnitude (M)). Properties of landslides characterised by long runouts onto glaciers are also difficult to extract because their runouts are seismically "quiet", likely due to frictional melting of glacier ice, causing underestimation of event duration and deposit size (Ekström and Stark, 2013). Despite these difficulties, current studies seem to indicate an increase in the rates of rock avalanching onto ice in rapidly deglaciating regions such as Alaska and the Southern Alps of New Zealand, where the
85 majority of recent (aseismic) RAs are associated with glaciers. This increase has been linked to climate warming (Huggel et al., 2012) and potential feedbacks with permafrost degradation (Allen et al., 2009; Coe et al., 2018; Krautblatter et al., 2013).

Here, we present the Google earth Engine supRaglAciaL Debris INput dEtector (GERALDINE): an open-access tool that utilises Google Earth Engine (GEE), and the Landsat data archive encompassing 37 years of optical imagery. The purpose of
90 the tool is to automatically delimit new supraglacial debris additions over wide areas and timescales, which then allows for rapid user-backed verification of inputs from large landslides specifically. GERALDINE is designed to allow quantification of the spatial and temporal underreporting of supraglacial rock avalanches. We describe the methods behind GERALDINE, verify tool outputs against known supraglacial inventories, and, finally demonstrate tool effectiveness by using it to find two new supraglacial rock avalanches, one of which cannot be found in the seismic archives.

95 **2.0   Method**

GERALDINE exploits the capability and large data archive of GEE (Gorelick et al., 2017), with all processing and data held in the cloud, removing the need to download raw data. By default, it utilises tier 1 Landsat imagery (30 m pixel resolution)

that has been converted to top-of-atmosphere (TOA) spectral reflectance (Chander et al., 2009), from 1984 – present, incorporating Landsat 4, 5, 7, and 8. GERALDINE also gives the user the following options: (i) to utilise tier 2 imagery; imagery that does not meet the same quality as tier 1, with geodetic accuracy > 12 m root mean square error (Dwyer et al., 2018); and (ii) to utilise real time Landsat imagery; imagery that uses preliminary geolocation and where thermal bands require additional processing, before the data is moved to its final imagery tier within 26 days for Landsat 7, and 16 days for Landsat 8. Tier 2 imagery is valuable in regions where tier 1 imagery is limited, e.g. Antarctica where there is a lack of ground control points for imagery geolocation. Real time imagery is useful for rapid identification of landslide locations if a seismic signal has been detected but an exact location has not been identified. Landsat imagery is used in conjunction with the Randolph Glacier Inventory (RGI) version 6.0 (RGI Consortium, 2017). The RGI is a global dataset of glacier outlines excluding those of the Greenland and Antarctic ice sheets, digitised both automatically and manually based on satellite imagery and local topographic maps (Pfeffer et al., 2014). RGI glacier boundaries are delineated from images acquired between 1943 and present day, potentially introducing errors into analysis due to outdated boundaries (Scherler et al., 2018) (see Supplementary Information Section 1.0). However, this database represents the best worldwide glacier inventory available and shrinking ice as the dominant global pattern means the tool is occasionally running over ice-free terrain with null results rather than missing potential supraglacial debris inputs. The RGI can be replaced by the user with shapefiles of the Greenland and Antarctic ice sheets, if analysis is required in these regions, or higher resolution (user defined) glacier outlines, if the RGI is deemed insufficient.

2.1 Overview of processing flow

GERALDINE gathers all Landsat images from the user-specified date range and the year preceding this user-specified date range within the user-specified region of interest (ROI), creating two image collections within GEE (we advise users to define ROIs <5000 km^2 and specify annual date ranges because large ROIs and date ranges can exceed GEE memory capacity). It clips all images to the ROI, applies a cloud mask, then a water mask, before finally delineating supraglacial debris cover from snow and ice. GERALDINE acquires the maximum debris extent from both image collections, creating two maximum debris mosaics, then subtracts these mosaics and clips them to the RGI v6.0 (or user defined area if not using RGI) to output a map. This map highlights debris within the user-specified time period that was not present in the preceding year, which we term 'new debris additions'. All files can be exported in GeoJSON (Georeferenced JavaScript Object Notation) format for further analysis, including to verify if detections are discrete landslide inputs. An overview of the workflow is presented in Figure 1 and the detail for each step described in Sections 2.1.1–2.1.4.

2.1.1 Cloud masking

GERALDINE masks cloud cover using the GEE built-in 'simple cloud score' function (Housman et al. 2018). This pixel-wise cloud probability score allows fast and efficient identification of clouds, suitable for large-scale analysis (Housman et al., 2018) and has been previously applied and well-justified for use in glacial environments (Scherler et al., 2018). A 20%

130   threshold is applied to every image, thereby excluding any pixel with a cloud score >20% from the image. We quantitatively

evaluated this threshold to ensure optimum tool performance (see Supporting Information Section 2.0). Cloud shadow is not

masked as it was found to have a minimal effect on the tool delineating debris from snow/ice whilst greatly increasing

processing time.

2.1.2 NDWI mask

135   Supraglacial streams and/or lakes are present on many glaciers worldwide (for full review see Pitcher and Smith, 2019).

GERALDINE includes a Normalised Difference Water Index (NDWI) (McFeeters, 1996) mask to omit these features from

debris detection. It utilises the green (0.52-0.6 λ) and near infrared (NIR) (0.76-0.9 λ) bands, the optimum band combination

for mountainous regions (Bolch et al., 2011). Other band combinations, such as the modified NDWI that employs the green

and shortwave infrared (SWIR) bands (Xu, 2006) as used in Watson et al. (2018), and the blue and NIR band (Huggel et al.,

140   2002), both struggle in the glacial regions we focus on (Chand and Watanabe, 2019; Gardelle et al., 2011). GERALDINE

employs a fixed NDWI threshold that was quantitatively evaluated against the glacial lake inventory of Wang et al. (2020),

masking values >0.4 as water (see Supplementary Information Section 3.0), similar to previous work on mountain glaciers

(Miles et al., 2017). Dynamic thresholding was unsuitable due to processing speed and memory constraints, and, importantly

for what the tool is designed to detect, it only offered marginal gains at significant processing and complexity cost.

145   ### 2.1.3 NDSI

The Normalised Difference Snow Index (NDSI) is a ratio calculated using the green (0.52-0.6 λ) and SWIR (1.55-1.75 λ)

bands. It helps distinguish snow/ice from other land cover (Hall et al., 1995) and excels at detecting ice where topographic

shading is commonplace (Racoviteanu et al., 2008) due to high reflectance in the visible range and strong absorption in the

SWIR range. GERALDINE applies the NDSI to all images and a threshold of 0.4 is used to create a binary image of

150   supraglacial debris (<0.4) and snow/ice (>0.4). This threshold has been utilised by studies in the Andes (e.g. Burns and Nolin,

2014) and Himalaya (e.g. Zhang et al., 2019), but optimum thresholds often vary between 0.5 (Gjermundsen et al., 2011) and

0.2 (Keshri et al., 2009; Kraaijenbrink et al., 2017). We justify our 0.4 value on Scherler et al. (2018) who used this threshold

to map and create a global supraglacial debris cover dataset using Landsat 8 images. GERALDINE is in effect standardised

with this global supraglacial cover map. We advise users to use this default threshold but if this appears sub-optimum in a user

155   defined region of interest (ROI), the threshold can be fine-tuned in the code (v1.0 line 264 and 274). We utilise NDSI instead

of newer band ratio techniques (e.g. Keshri et al., 2009) and more complex algorithms (e.g. Bhardwaj et al., 2015) to ensure

transferability between Landsat TM, ETM+ and OLI TIRS sensors as we wish to harness the full temporal archive.

2.1.4 Retrieving maximum debris extent

To attain a maximum debris extent, GERALDINE reduces each image collection to an individual image using a pixel-based
approach (Fig. 2). Every binary image (supraglacial debris: 0, snow/ice: 1) in each image collection is stacked, with pixels in
the same geographic location stacked sequentially. If any pixel in the temporal image stack is debris, the corresponding pixel
in the final mosaic will be a debris pixel, creating a maximum debris extent mosaic. GERALDINE is therefore debris biased
due to this processing step. Calculated maximum debris extent mosaics for both the user-defined time period and previous year
are differenced, the output being new debris additions. Both the previous year maximum debris extent, and new debris addition
mosaics, are displayed for user analysis within the GEE interactive development environment, and easily exportable to Google
Drive (included as part of sign-up to Google Earth Engine).

2.2 Validation

A bipartite validation was undertaken to assess the effectiveness of GERALDINE outputs for allowing a user to rapidly identify
supraglacially deposited RAs: a detection validation (i.e. can the user confirm a rock avalanche has occurred from a
GERALDINE output?), and an area validation (i.e. how much of the area of the RA has GERALDINE detected?). Although
areal detection is not the main purpose of the tool, greater area detection would ultimately help the user in RA identification.
Validation was performed against the supraglacially deposited rock avalanche (RA) databases of Bessette-Kirton and Coe
(2016), Deline et al. (2014), Uhlmann et al. (2013) and the Exotic Seismic Events Catalog (IRIS DMC, 2017). To provide
validation, large supraglacial debris additions had to occur after 1984 (onset of Landsat TM era) and had to deposit debris
predominantly onto clean-ice areas of glaciers in the RGI. Forty-eight suitable events were found, their locations distributed
across the European Alps, Alaska, New Zealand, Canada, Russia and Iceland.

GERALDINE was run for the year of the event using Landsat tier 1 imagery; the new debris vector output file was exported
into a GIS and after an initial qualitative step to see if the user would flag the RA from the GERALDINE output, the area of
the deposit it detected was calculated. The tool-detected area was compared against an outline of the RA manually-digitised
from a Landsat image using the Google Earth Engine Digitisation Tool (GEEDiT) (Lea, 2018). These two steps allow for an
assessment of GERALDINEs ability to highlight new debris inputs, and if this changes over the Landsat era.

3.0   Results and Discussion

3.1 Validation

GERALDINE outputs allowed user identification of 92 % of all validation RAs. False negatives all pre-date 1991 (Figure 3),
and can be explained by a failure of Landsat satellites from imaging the RA deposit, due to reduced (and insufficient in this
case) tier 1 Landsat image availability pre-Landsat 7 within the GEE data catalogue, inhibiting GERALDINE from
highlighting the RA as new debris. We note that if just one image featured the RA, GERALDINE would highlight the deposit

as new debris due to its bias towards debris detection (see section 2.1.4). A true 100 % detection rate for RA events on glaciers
190 is, however, unlikely, due to some deposits having high snow/ice content or entraining large amounts of snow/ice during
events, which can be common for rock avalanches deposited onto glaciers. This high snow/ice content can mask them as
snow/ice during NDSI delineation from debris, inhibiting detection. However, events of this kind also pose significant
difficulty for user delineation with original optical imagery. GERALDINE works best when a number of images in the image
stack represent maximal debris cover in the preceding year, reducing false positives for the timespan of interest i.e. flagging
195 old debris as new debris, due to a lack of old debris exposure in the previous year. This is particularly applicable to small (<0.5
km^2) glaciers, where the accuracy of medium resolution satellite imagery is lower (Paul et al., 2013). The debris bias of
GERALDINE ensures true negative detection is also extremely high, but this high true negative detection is why user
verification of new debris outputs is needed, because they are flagged as new debris but display no supraglacial RA
characteristics i.e. lobate and elongated (Deline et al., 2014). To a user familiar with glacial and landslide processes, the
200 differences in GERALDINE outputs between true positives/negatives and false positives/negatives are clear when running the
tool to find RA inputs.

GERALDINE RA areal accuracy increases over time from 19 % in the Landsat 4/5 era, to 71 % with the current Landsat 7/8
constellation (Fig. 3), with the latter period characterised by increasingly modern sensors with greater spectral and temporal
205 resolution. Low areal accuracy in the Landsat 4/5 era is once again a product of the GEE data catalogue having limited imagery
for certain years in glaciated areas, reducing the ability of GERALDINE to detect the entire area of new debris additions. Areal
accuracy increases after the failure of Landsat 4 in December 1993, at which point Landsat 5 is the sole data collector of
imagery at a frequency of every 16 days. Despite this single functioning satellite, the tool detects all eight validation events
and on average 59 % of the deposit areas between 1993 and the activation of Landsat 7 in 1999. The dual Landsat 5/7
210 constellation increases tool area accuracy further to 69 %. However, a decrease in mean area accuracy is evident after the
failure of the Landsat 7 Scan Line Corrector (SLC) in May 2003 (Markham et al., 2004), decreasing tool areal accuracy by 4
%, due to images missing up to 20-25 % of data per image in the stack (Hossain et al., 2015). We find that a number of Landsat
7 scenes also feature stripes of no data, pre-dating the SLC failure, and can inaccurately cause 'stripes' of new debris in tool
outputs. The current Landsat 7/8 constellation has the highest accuracy for detecting the area of RAs at 71 %. The smallest
215 new debris addition we used for validation was 0.062 km^2, of which GERALDINE detected 71 % of the area, so we have
confidence in detection greater than 0.05 km^2, equating to ~56 Landsat pixels. Even with GERALDINE performing well,
additional refinement and/or full automation of RA identification would be an interesting, and priority, area for further
investigation.

220 GERALDINE is frequently affected by the RGI dataset causing over/under-estimation of previous year debris extents and new
debris additions. For example, at tidewater glaciers that have undergone retreat since their margins were digitised, the tool
often detects clean ice and debris at the tongue. This is solely dependent on the presence of ice mélange in imagery, and NDWI

masking struggling to mask fjord water due to its optimization for masking supraglacial ponds (see Supporting Information Section 1.0 and 3.0). In addition, we found an instance where a supraglacial rock avalanche deposit had been misclassified as a nunatak (60°27'23.7"N, 142°33'35.7"W) and therefore this section of the glacier is erroneously missing from the RGI dataset altogether, preventing tool detection, but this is likely a single case. Topographic shading on debris cover can at times cause pixels to be masked from Landsat scenes due to misclassification as supraglacial water and/or cloud; however, if the tool is run over a sufficiently long period, this will not influence new debris detection.

3.2 New Supraglacial Input Detection Example

The Hayes Range, Alaska has a history of large supraglacial debris additions (e.g. Jibson et al., 2006), but no events have been documented in the last decade, in contrast to a recent dense cluster in the Glacier Bay area of Alaska (Coe et al., 2018), which formed part of the validation dataset. To test this, we ran GERALDINE for 2018 to highlight new debris additions on glaciers in the Hayes Range (Fig. 4a). The output map highlighted two large RAs deposited onto glaciers between 1 January 2018 and 31 December 2018. These were manually verified and the potential window of event occurrence identified using satellite imagery within GeeDiT (Lea, 2018). The larger of the two RAs is from a slope collapse on the southern flank of Mt Hayes (4216 m) (63°35'11.7"N, 146°42'50.0"W), with emplacement determined between 10 and 25 February 2018 (Fig. 4b). This rock avalanche was also detected using the seismic method (Ekström and Stark, 2013 see Section 1.0), and confirmed as occurring on 12 February 2018 (Goran Ekström, personal communication, 2019). The resulting debris deposit covered 9.3 km^2 of the surface of the Susitna Glacier (digitised from Planet Labs Inc. imagery from 31/07/2018). The tool detected 27.5 % of the area of this RA, due to emplacement predominantly in the accumulation area, with the upper half of the deposit rapidly covered by snow after the event. The second, smaller RA occurred between 4 and 7 July 2018, on an unnamed glacier to the east of Maclaren Glacier (63°20'21.9"N, 146°26'36.1"W) (Fig. 4c). GERALDINE detected 78 % of this 2.01 km^2 supraglacial debris input, which transformed the glacier from 28 % debris covered to 72 % debris covered, and will have important implications for glacier melt regime, velocity and response to atmospheric drivers. Unlike the larger RA from Mt Hayes, this event was not automatically detected using seismic methods (Goran Ekström, personal communication, 2019), suggesting that its seismic signature was lower than the seismic detection limit (M < 5.0) (Ekström and Stark, 2013). Therefore, there is a high potential to detect all events using GERALDINE, and then provide time-location filters to seismic records to retrospectively quantify force histories and precise timings of events not flagged automatically as a landslide.

We note that new large debris inputs are partially highlighted on the Black Rapids Glacier for 2018 (Fig. 4d), but these 'new' additions were actually deposited in 2002 during the Denali earthquake (Jibson et al., 2006; Shugar et al., 2012; Shugar and Clague, 2011). We assign this discrepancy to minimal cloud-free imagery during summer (a time when deposits are uncovered by snow melt), preventing the tool from highlighting their full summer extent, and causing underestimation of the 2017 debris cover. To a human operator, however, it is clear these debris additions are erroneous because 'new' debris is patchy, with 2017

255 debris extent and snow/ice preventing detection of a homogeneous deposit. When GERALDINE is run for multiple years
sequentially in the area, the user will have already determined the date of these earlier supraglacial landslides.

3.3 Tracking new debris transportation

A secondary use of GERALDINE is tracking existing debris. For example, large supraglacially deposited RAs are transported
down-glacier, although often the initial emplacement geometry is characteristically deformed and spread due to differential
260 ablation and ice motion (Reznichenko et al., 2011; Uhlmann et al., 2013). The tool can give an indication of this movement,
by highlighting new debris at the down-glacier end of the deposit and differencing the distance of this new debris from the
previous year's deposit extent. This gives an indication of deposit behaviour, transient residence time, and glacier velocity,
which is often unknown at the temporal resolution of Landsat and complex to calculate in high mountain regions (Sam et al.,
2015).

265

To demonstrate the evolution of a RA through time, we ran GERALDINE for 2012, 2013, and 2014 for the Lituya Mountain
RA in Alaska. This RA occurred on 11 June 2012 and was deposited onto a tributary of the John Hopkins glacier (Geertsema,
2012). The upper portion of the deposit was sequestered into the ice after its deposition in 2012, as is common of debris inputs
in glacier accumulation areas (Dunning et al., 2015). However, the deposit toe remained visible on the surface, likely because
270 it was below the snow line. We estimate the down-glacier transport velocity of this RA by tracking and measuring the
movement of the deposit toe, to measure the displacement of the deposit leading edge. Using this method, estimates of down-
glacier transportation of the deposit leading edge between 2012 and 2013 are ~575 ± 30 m, and ~328 ± 30 m between 2013
and 2014 (Fig. 5), the latter in agreement with glacier velocity calculated by Burgess et al. (2013) between 2007 and 2010 (250
– 350 m a^{-1}), and ITS_LIVE velocity from 2013 (300-400 m a^{-1}) (Gardner et al., 2018; Gardner et al., 2019). We suggest that
275 the higher RA deposit velocities between 2012 and 2013 are a result of the immediate response of the glacier to reduced
ablation rates and, expansion of debris surface coverage as the RA deposit was redistributed off the protected ice-pedestal
formed beneath (Reznichenko et al., 2011).

4.0 Conclusion

GERALDINE is the first open-access resource that can rapidly highlight new supraglacial debris additions onto clean ice for
280 a user-specified time and location. Using the output maps it produces, it gives an objective starting point from which a user
can identify new debris inputs, eliminating the time-intensive process of manually downloading, processing and inspecting
numerous satellite images. We demonstrate its effectiveness by verifying it against 48 known, large, supraglacially deposited
rock avalanches that occurred in North America, Europe, Asia, and New Zealand. GERALDINE outputs helped identify 92%
of all 48 events, with 100% successful identification post-1991 when image quality and availability increases. We showcase
285 how GERALDINE outperforms current methods that assist with user identification of large debris additions, by identifying

two new glacial rock avalanches in 2018, in the Hayes Range of Alaska, one of which could not be detected using current methods. Therefore, the frequency of large supraglacial debris inputs is likely historically underestimated. GERALDINE can become part of the repertoire of tools that enable glacial rock avalanches/landslides to be identified in the past, present, and future. It will improve remote detection and characterisation of these events, to help quantify and evaluate their frequency,

290   spatial distribution and long-term behaviour in a changing climate.

Code/data availability

GERALDINE code and the validation dataset are available at https://doi.org/10.5281/zenodo.3524414. All other results can be recreated by running GERALDINE in the respective example areas. A guide on how to use GERALDINE is provided in Supplementary Information Section 4.0.

295   **Author responsibilities**

WS developed the tool and wrote the manuscript. SD made substantial contributions to the conception and functionality of the tool, as well as manuscript editing. NR, SB and JT provided useful guidance on tool functionality and contributed to the manuscript.

Acknowledgments

300   This work was funded by a Newcastle University Research Excellence Award PhD scholarship to W. Smith. We acknowledge the freely available Landsat datasets provided by the USGS and hosted in the Google Earth Engine data catalogue, and the Randolph Glacier Inventory v6.0 (RGI Consortium, 2017). Hillshade IFSAR DTMs used for figure production were collected as part of the Alaska Mapping Initiative (doi:10.5066/P9C064CO) and are available through the USGS EarthExplorer data portal. We would also like to thank Ryan Dick for his feedback on early versions of GERALDINE.

305   **Competing interests**

The authors declare that they have no conflict of interests.

References

Akhtar, M., Ahmad, N. and Booij, M. J.: The impact of climate change on the water resources of Hindukush-Karakorum-Himalaya region under different glacier coverage scenarios, J. Hydrol., 355(1–4), 148–163, doi:10.1016/j.jhydrol.2008.03.015,
310   2008.

Allen, S. K., Gruber, S. and Owens, I. F.: Exploring steep bedrock permafrost and its relationship with recent slope failures in the southern alps of New Zealand, Permafr. Periglac. Process., 20(4), 345–356, doi:10.1002/ppp.658, 2009.

Allen, S. K., Cox, S. C. and Owens, I. F.: Rock avalanches and other landslides in the central Southern Alps of New Zealand: A regional study considering possible climate change impacts, Landslides, 8(1), 33–48, doi:10.1007/s10346-010-0222-z, 2011.

315   Ballantyne, C. K.: A general model of paraglacial landscape response, Holocene, 12(3), 371–376, doi:10.1191/0959683602hl553fa, 2002.

Ballantyne, C. K., Wilson, P., Gheorghiu, D. and Rodés, À.: Enhanced rock-slope failure following ice-sheet deglaciation: Timing and causes, Earth Surf. Process. Landforms, 39(7), 900–913, doi:10.1002/esp.3495, 2014a.

Ballantyne, C. K., Sandeman, G. F., Stone, J. O. and Wilson, P.: Rock-slope failure following Late Pleistocene deglaciation
320   on tectonically stable mountainous terrain, Quat. Sci. Rev., 86, 144–157, doi:10.1016/j.quascirev.2013.12.021, 2014b.

Benn, D. I., Bolch, T., Hands, K., Gulley, J., Luckman, A., Nicholson, L. I., Quincey, D., Thompson, S., Toumi, R. and Wiseman, S.: Response of debris-covered glaciers in the Mount Everest region to recent warming, and implications for outburst flood hazards, Earth-Science Rev., 114(1–2), 156–174, doi:10.1016/j.earscirev.2012.03.008, 2012.

Berthier, E., Schiefer, E., Clarke, G. K. C., Menounos, B. and Rémy, F.: Contribution of Alaskan glaciers to sea-level rise
325   derived from satellite imagery, Nat. Geosci., 3(2), 92–95, doi:10.1038/ngeo737, 2010.

Bessette-Kirton, E.K. and Coe, J.A.: Inventory of rock avalanches in western Glacier Bay National Park and Preserve, Alaska, 1984-2016: a baseline data set for evaluating the impact of climate change on avalanche magnitude, mobility, and frequency, U.S. Geological Survey data release, doi:10.5066/F7C827F8, 2016.

Bhardwaj, A., Joshi, P. K., Snehmani, Sam, L., Singh, M. K., Singh, S. and Kumar, R.: Applicability of Landsat 8 data for
330   characterizing glacier facies and supraglacial debris, Int. J. Appl. Earth Obs. Geoinf., 38, 51–64, doi:10.1016/j.jag.2014.12.011, 2015.

Bhutiyani, M. R. and Mahto, R.: Remote-sensing-based study of impact of a rock avalanche on North Terong Glacier in Karakorum Himalaya, Int. J. Remote Sens., 39(22), 8076–8091, doi:10.1080/01431161.2018.1480073, 2018.

Blöthe, J. H., Korup, O. and Schwanghart, W.: Large landslides lie low: Excess topography in the Himalaya-Karakoram ranges,
335   Geology, 43(6), 523–526, doi:10.1130/G36527.1, 2015.

Bolch, T., Peters, J., Yegorov, A., Pradhan, B., Buchroithner, M. and Blagoveshchensky, V.: Identification of potentially dangerous glacial lakes in the northern Tien Shan, Nat. Hazards, 59(3), 1691–1714, doi:10.1007/s11069-011-9860-2, 2011.

Burgess, E. W., Forster, R. R. and Larsen, C. F.: Flow velocities of Alaskan glaciers, Nat. Commun., 4(1), 2146, doi:10.1038/ncomms3146, 2013.

340   Burns, P. and Nolin, A.: Using atmospherically-corrected Landsat imagery to measure glacier area change in the Cordillera Blanca, Peru from 1987 to 2010, Remote Sens. Environ., 140, 165–178, doi:10.1016/j.rse.2013.08.026, 2014.

Chand, M. B. and Watanabe, T.: Development of Supraglacial Ponds in the Everest Region, Nepal, between 1989 and 2018, Remote Sens., 11(9), 1058, doi:10.3390/rs11091058, 2019.

Chander, G., Markham, B. L. and Helder, D. L.: Summary of current radiometric calibration coefficients for Landsat MSS,

345   TM, ETM+, and EO-1 ALI sensors, Remote Sens. Environ., 113(5), 893–903, doi:10.1016/j.rse.2009.01.007, 2009.

Coe, J. A., Bessette-Kirton, E. K. and Geertsema, M.: Increasing rock-avalanche size and mobility in Glacier Bay National Park and Preserve, Alaska detected from 1984 to 2016 Landsat imagery, Landslides, 15(3), 393–407, doi:10.1007/s10346-017-0879-7, 2018.

Deline, P., Hewitt, K., Reznichenko, N. and Shugar, D.: Rock Avalanches onto Glaciers, in Landslide Hazards, Risks, and

350   Disasters, pp. 263–319, Academic Press., 2014.

Dufresne, A., Wolken, G. J., Hibert, C., Bessette-Kirton, E. K., Coe, J. A., Geertsema, M. and Ekström, G.: The 2016 Lamplugh rock avalanche, Alaska: deposit structures and emplacement dynamics, Landslides, 1–19, doi:10.1007/s10346-019-01225-4, 2019.

Dunning, S. A., Rosser, N. J., McColl, S. T. and Reznichenko, N. V.: Rapid sequestration of rock avalanche deposits within

355   glaciers, Nat. Commun., 6, 7964, doi:10.1038/ncomms8964, 2015.

Dwyer, J. L., Roy, D. P., Sauer, B., Jenkerson, C. B., Zhang, H. K. and Lymburner, L.: Analysis ready data: Enabling analysis of the landsat archive, Remote Sens., 10(9), 1363, doi:10.3390/rs10091363, 2018.

Ekström, G. and Stark, C. P.: Simple scaling of catastrophic landslide dynamics, Science (80-.)., 339(6126), 1416–1419, doi:10.1126/science.1232887, 2013.

360   Fyffe, C. L., Brock, B. W., Kirkbride, M. P., Mair, D. W. F., Arnold, N. S., Smiraglia, C., Diolaiuti, G. and Diotri, F.: Do debris-covered glaciers demonstrate distinctive hydrological behaviour compared to clean glaciers?, J. Hydrol., 570, 584–597, doi:10.1016/j.jhydrol.2018.12.069, 2019.

Gardelle, J., Arnaud, Y. and Berthier, E.: Contrasted evolution of glacial lakes along the Hindu Kush Himalaya mountain range between 1990 and 2009, Glob. Planet. Change, 75(1–2), 47–55, doi:10.1016/J.GLOPLACHA.2010.10.003, 2011.

365   Gardner, A. S., Moholdt, G., Scambos, T., Fahnstock, M., Ligtenberg, S., van den Broeke, M. and Nilsson, J.: Increased West Antarctic and unchanged East Antarctic ice discharge over the last 7 years, Cryosph., 12(2), 521–547, doi:10.5194/tc-12-521-2018, 2018.

Gardner, A. S., Fahnestock, M. A. and Scambos, T. A.: ITS_LIVE Regional Glacier and Ice Sheet Surface Velocities. Data archived at National Snow and Ice Data Center, doi:10.5067/6II6VW8LLWJ7, 2019.

370   Geertsema, M.: Initial observations of the 11 June 2012 rock / ice avalanche , Lituya, in The First Meeting of Cold Region Landslides Network, Harbin, China, pp. 1–5., 2012.

Gjermundsen, E. F., Mathieu, R., Kääb, A., Chinn, T., Fitzharris, B. and Hagen, J. O.: Assessment of multispectral glacier mapping methods and derivation of glacier area changes, 1978-2002, in the central Southern Alps, New Zealand, from ASTER satellite data, field survey and existing inventory data, J. Glaciol., 57(204), 667–683, doi:10.3189/002214311797409749, 2011.

375   Gorelick, N., Hancher, M., Dixon, M., Ilyushchenko, S., Thau, D. and Moore, R.: Google Earth Engine: Planetary-scale geospatial analysis for everyone, Remote Sens. Environ., 202, 18–27, doi:10.1016/j.rse.2017.06.031, 2017.

Grämiger, L. M., Moore, J. R., Gischig, V. S., Ivy-Ochs, S. and Loew, S.: Beyond debuttressing: Mechanics of paraglacial rock slope damage during repeat glacial cycles, J. Geophys. Res. Earth Surf., 122(4), 1004–1036, doi:10.1002/2016JF003967,

2017.

380 Hall, D. K., Riggs, G. A. and Salomonson, V. V.: Development of methods for mapping global snow cover using moderate resolution imaging spectroradiometer data, Remote Sens. Environ., 54(2), 127–140, doi:10.1016/0034-4257(95)00137-P, 1995.

Hewitt, K.: Quaternary moraines vs catastrophic rock avalanches in the Karakoram Himalaya, Northern Pakistan, Quat. Res., 51(3), 220–237, doi:10.1006/qres.1999.2033, 1999.

385 Hewitt, K.: Rock avalanches that travel onto glaciers and related developments, Karakoram Himalaya, Inner Asia, Geomorphology, 103(1), 66–79, doi:10.1016/j.geomorph.2007.10.017, 2009.

Hossain, M. S., Bujang, J. S., Zakaria, M. H. and Hashim, M.: Assessment of Landsat 7 Scan Line Corrector-off data gap-filling methods for seagrass distribution mapping, Int. J. Remote Sens., 36(4), 1188–1215, doi:10.1080/01431161.2015.1007257, 2015.

390 Housman, I. W., Chastain, R. A. and Finco, M. V.: An evaluation of forest health insect and disease survey data and satellite-based remote sensing forest change detection methods: Case studies in the United States, Remote Sens., 10(8), 1184, doi:10.3390/rs10081184, 2018.

Huggel, C., Kääb, A., Haeberli, W., Teysseire, P. and Paul, F.: Remote sensing based assessment of hazards from glacier lake outbursts: a case study in the Swiss Alps, Can. Geotech. J., 39(2), 316–330, doi:10.1139/t01-099, 2002.

395 Huggel, C., Clague, J. J. and Korup, O.: Is climate change responsible for changing landslide activity in high mountains?, Earth Surf. Process. Landforms, 37(1), 77–91, doi:10.1002/esp.2223, 2012.

IRIS DMC: Data Services Products: Exotic Seismic Events Catalog, doi:10.17611/DP/ESEC.1, 2017.

Jamieson, S. S. R., Ewertowski, M. W. and Evans, D. J. A.: Rapid advance of two mountain glaciers in response to mine-related debris loading, J. Geophys. Res. Earth Surf., 120(7), 1418–1435, doi:10.1002/2015JF003504, 2015.

400 Jarman, D. and Harrison, S.: Rock slope failure in the British mountains, Geomorphology, 340, 202–233, doi:10.1016/j.geomorph.2019.03.002, 2019.

Jibson, R. W., Harp, E. L., Schulz, W. and Keefer, D. K.: Large rock avalanches triggered by the M 7.9 Denali Fault, Alaska, earthquake of 3 November 2002, Eng. Geol., 83(1–3), 144–160, doi:10.1016/j.enggeo.2005.06.029, 2006.

Keshri, A. K., Shukla, A. and Gupta, R. P.: ASTER ratio indices for supraglacial terrain mapping, Int. J. Remote Sens., 30(2),
405 519–524, doi:10.1080/01431160802385459, 2009.

Kirkbride, M. P. and Deline, P.: The formation of supraglacial debris covers by primary dispersal from transverse englacial debris bands, Earth Surf. Process. Landforms, 38(15), 1779–1792, doi:10.1002/esp.3416, 2013.

Kraaijenbrink, P. D. A., Bierkens, M. F. P., Lutz, A. F. and Immerzeel, W. W.: Impact of a global temperature rise of 1.5 degrees Celsius on Asia's glaciers, Nature, 549(7671), 257–260, doi:10.1038/nature23878, 2017.

410 Krautblatter, M., Funk, D. and Günzel, F. K.: Why permafrost rocks become unstable: A rock-ice-mechanical model in time and space, Earth Surf. Process. Landforms, 38(8), 876–887, doi:10.1002/esp.3374, 2013.

Lea, J. M.: The Google Earth Engine Digitisation Tool (GEEDiT) and the Margin change Quantification Tool (MaQiT) -

Simple tools for the rapid mapping and quantification of changing Earth surface margins, Earth Surf. Dyn., 6(3), 551–561, doi:10.5194/esurf-6-551-2018, 2018.

415   Mackay, S. L., Marchant, D. R., Lamp, J. L. and Head, J. W.: Cold-based debris-covered glaciers: Evaluating their potential as climate archives through studies of ground-penetrating radar and surface morphology, J. Geophys. Res. F Earth Surf., 119(11), 2505–2540, doi:10.1002/2014JF003178, 2014.

Markham, B. L., Storey, J. C., Williams, D. L. and Irons, J. R.: Landsat sensor performance: History and current status, IEEE Trans. Geosci. Remote Sens., 42(12), 2691–2694, doi:10.1109/TGRS.2004.840720, 2004.

420   McFeeters, S. K.: The use of the Normalized Difference Water Index (NDWI) in the delineation of open water features, Int. J. Remote Sens., 17(7), 1425–1432, doi:10.1080/01431169608948714, 1996.

Mihalcea, C., Mayer, C., Diolaiuti, G., D'Agata, C., Smiraglia, C., Lambrecht, A., Vuillermoz, E. and Tartari, G.: Spatial distribution of debris thickness and melting from remote-sensing and meteorological data, at debris-covered Baltoro glacier, Karakoram, Pakistan, in Annals of Glaciology, vol. 48, pp. 49–57, Cambridge University Press., 2008a.

425   Mihalcea, C., Brock, B. W., Diolaiuti, G., D'Agata, C., Citterio, M., Kirkbride, M. P., Cutler, M. E. J. and Smiraglia, C.: Using ASTER satellite and ground-based surface temperature measurements to derive supraglacial debris cover and thickness patterns on Miage Glacier (Mont Blanc Massif, Italy), Cold Reg. Sci. Technol., 52(3), 341–354, doi:10.1016/j.coldregions.2007.03.004, 2008b.

Miles, E. S., Willis, I. C., Arnold, N. S., Steiner, J. and Pellicciotti, F.: Spatial, seasonal and interannual variability of
430   supraglacial ponds in the Langtang Valley of Nepal, 1999-2013, J. Glaciol., 63(237), 88–105, doi:10.1017/jog.2016.120, 2017.

Nicholson, L. and Benn, D. I.: Calculating ice melt beneath a debris layer using meteorological data, J. Glaciol., 52(178), 463–470, doi:10.3189/172756506781828584, 2006.

Östrem, G.: Ice Melting under a Thin Layer of Moraine, and the Existence of Ice Cores in Moraine Ridges, Geogr. Ann., 41(4), 228–230 [online] Available from: http://www.jstor.org/stable/4626805, 1959.

435   Pánek, T., Mentlík, P., Engel, Z., Braucher, R. and Zondervan, A.: Late Quaternary sackungen in the highest mountains of the Carpathians, Quat. Sci. Rev., 159, 47–62, doi:10.1016/j.quascirev.2017.01.008, 2017.

Paul, F., Barrand, N. E., Baumann, S., Berthier, E., Bolch, T., Casey, K., Frey, H., Joshi, S. P., Konovalov, V., Le Bris, R., Mölg, N., Nosenko, G., Nuth, C., Pope, A., Racoviteanu, A., Rastner, P., Raup, B., Scharrer, K., Steffen, S. and Winsvold, S.: On the accuracy of glacier outlines derived from remote-sensing data, Ann. Glaciol., 54(63), 171–182,
440   doi:10.3189/2013AoG63A296, 2013.

Pfeffer, W. T., Arendt, A. A., Bliss, A., Bolch, T., Cogley, J. G., Gardner, A. S., Hagen, J.-O., Hock, R., Kaser, G., Kienholz, C., Miles, E. S., Moholdt, G., Mölg, N., Paul, F., Radić, V., Rastner, P., Raup, B. H., Rich, J. and Sharp, M. J.: The Randolph Glacier Inventory: a globally complete inventory of glaciers, J. Glaciol., 60(221), 537–552, doi:10.3189/2014jog13j176, 2014.

Pitcher, L. H. and Smith, L. C.: Supraglacial Streams and Rivers, Annu. Rev. Earth Planet. Sci., 47(1), 421–452,
445   doi:10.1146/annurev-earth-053018-060212, 2019.

Porter, P. R., Vatne, G., Ng, F. and Irvine-Fynn, T. D. L.: Ice-marginal sediment delivery to the surface of a high-arctic glacier:

Austre brøggerbreen, svalbard, Geogr. Ann. Ser. A Phys. Geogr., 92(4), 437–449, doi:10.1111/j.1468-0459.2010.00406.x, 2010.

Racoviteanu, A. E., Arnaud, Y., Williams, M. W. and Ordoñez, J.: Decadal changes in glacier parameters in the Cordillera
450 Blanca, Peru, derived from remote sensing, J. Glaciol., 54(186), 499–510, doi:10.3189/002214308785836922, 2008.

Reznichenko, N., Davies, T., Shulmeister, J. and McSaveney, M.: Effects of debris on ice-surface melting rates: An experimental study, J. Glaciol., 56(197), 384–394, doi:10.3189/002214310792447725, 2010.

Reznichenko, N. V., Davies, T. R. H. and Alexander, D. J.: Effects of rock avalanches on glacier behaviour and moraine formation, Geomorphology, 132(3–4), 327–338, doi:10.1016/j.geomorph.2011.05.019, 2011.

455 RGI Consortium: Randolph Glacier Inventory – A Dataset of Global Glacier Outlines: Version 6.0: Technical Report, Global Land Ice Measurements from Space, Colorado, USA. Digital Media. doi:10.7265/N5-RGI-60, 2017.

Sam, L., Bhardwaj, A., Singh, S. and Kumar, R.: Remote sensing flow velocity of debris-covered glaciers using Landsat 8 data, Prog. Phys. Geogr., 40(2), 305–321, doi:10.1177/0309133315593894, 2015.

Sanhueza-Pino, K., Korup, O., Hetzel, R., Munack, H., Weidinger, J. T., Dunning, S., Ormukov, C. and Kubik, P. W.: Glacial
460 advances constrained by 10Be exposure dating of bedrock landslides, Kyrgyz Tien Shan, Quat. Res., 76(3), 295–304, doi:10.1016/j.yqres.2011.06.013, 2011.

Scherler, D., Bookhagen, B. and Strecker, M. R.: Hillslope-glacier coupling: The interplay of topography and glacial dynamics in High Asia, J. Geophys. Res. Earth Surf., 116(2), doi:10.1029/2010JF001751, 2011a.

Scherler, D., Bookhagen, B. and Strecker, M. R.: Spatially variable response of Himalayan glaciers to climate change affected
465 by debris cover, Nat. Geosci., 4(3), 156–159, doi:10.1038/ngeo1068, 2011b.

Scherler, D., Wulf, H. and Gorelick, N.: Global Assessment of Supraglacial Debris-Cover Extents, Geophys. Res. Lett., 45(21), 11,798-11,805, doi:10.1029/2018GL080158, 2018.

Shugar, D. H. and Clague, J. J.: The sedimentology and geomorphology of rock avalanche deposits on glaciers, Sedimentology, 58(7), 1762–1783, doi:10.1111/j.1365-3091.2011.01238.x, 2011.

470 Shugar, D. H., Rabus, B. T., Clague, J. J. and Capps, D. M.: The response of Black Rapids Glacier, Alaska, to the Denali earthquake rock avalanches, J. Geophys. Res. Earth Surf., 117(1), n/a-n/a, doi:10.1029/2011JF002011, 2012.

Shulmeister, J., Davies, T. R., Evans, D. J. A., Hyatt, O. M. and Tovar, D. S.: Catastrophic landslides, glacier behaviour and moraine formation - A view from an active plate margin, Quat. Sci. Rev., 28(11–12), 1085–1096, doi:10.1016/j.quascirev.2008.11.015, 2009.

475 Tielidze, L. G., Bolch, T., Wheate, R. D., Kutuzov, S. S., Lavrentiev, I. I. and Zemp, M.: Supra-glacial debris cover changes in the Greater Caucasus from 1986 to 2014, Cryosph., 14(2), 585–598, doi:10.5194/tc-14-585-2020, 2020.

Tovar, D. S., Shulmeister, J. and Davies, T. R.: Evidence for a landslide origin of New Zealand's Waiho Loop moraine, Nat. Geosci., 1(8), 524–526, doi:10.1038/ngeo249, 2008.

Uhlmann, M., Korup, O., Huggel, C., Fischer, L. and Kargel, J. S.: Supra-glacial deposition and flux of catastrophic rock-slope
480 failure debris, south-central Alaska, Earth Surf. Process. Landforms, 38(7), 675–682, doi:10.1002/esp.3311, 2013.

Vacco, D. A., Alley, R. B. and Pollard, D.: Glacial advance and stagnation caused by rock avalanches, Earth Planet. Sci. Lett., 294(1–2), 123–130, doi:10.1016/j.epsl.2010.03.019, 2010.

Wang, X., Guo, X., Yang, C., Liu, Q., Wei, J., Zhang, Y., Liu, S., Zhang, Y., Jiang, Z. and Tang, Z.: Glacial lake inventory of High Mountain Asia (1990–2018) derived from Landsat images, Earth Syst. Sci. Data Discuss., (January), 1–23, doi:10.5194/essd-2019-212, 2020.

Watson, C. S., King, O., Miles, E. S. and Quincey, D. J.: Optimising NDWI supraglacial pond classification on Himalayan debris-covered glaciers, Remote Sens. Environ., 217, 414–425, doi:10.1016/J.RSE.2018.08.020, 2018.

Wirbel, A., Jarosch, A. H. and Nicholson, L.: Modelling debris transport within glaciers by advection in a full-Stokes ice flow model, Cryosphere, 12(1), 189–204, doi:10.5194/tc-12-189-2018, 2018.

Van Woerkom, T., Steiner, J. F., Kraaijenbrink, P. D. A., Miles, E. S. and Immerzeel, W. W.: Sediment supply from lateral moraines to a debris-covered glacier in the Himalaya, Earth Surf. Dyn., 7(2), 411–427, doi:10.5194/esurf-7-411-2019, 2019.

Xu, H.: Modification of normalised difference water index (NDWI) to enhance open water features in remotely sensed imagery, Int. J. Remote Sens., 27(14), 3025–3033, doi:10.1080/01431160600589179, 2006.

Zhang, J., Jia, L., Menenti, M. and Hu, G.: Glacier Facies Mapping Using a Machine-Learning Algorithm: The Parlung Zangbo Basin Case Study, Remote Sens., 11(4), 452, doi:10.3390/rs11040452, 2019.
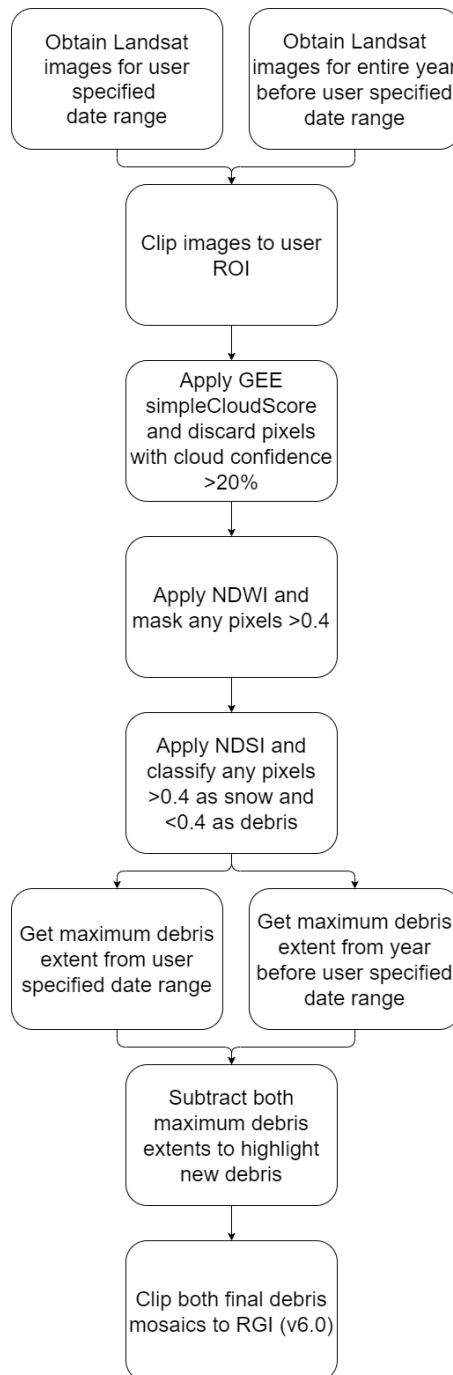
Figure 1: Processing flow of GERALDINE.
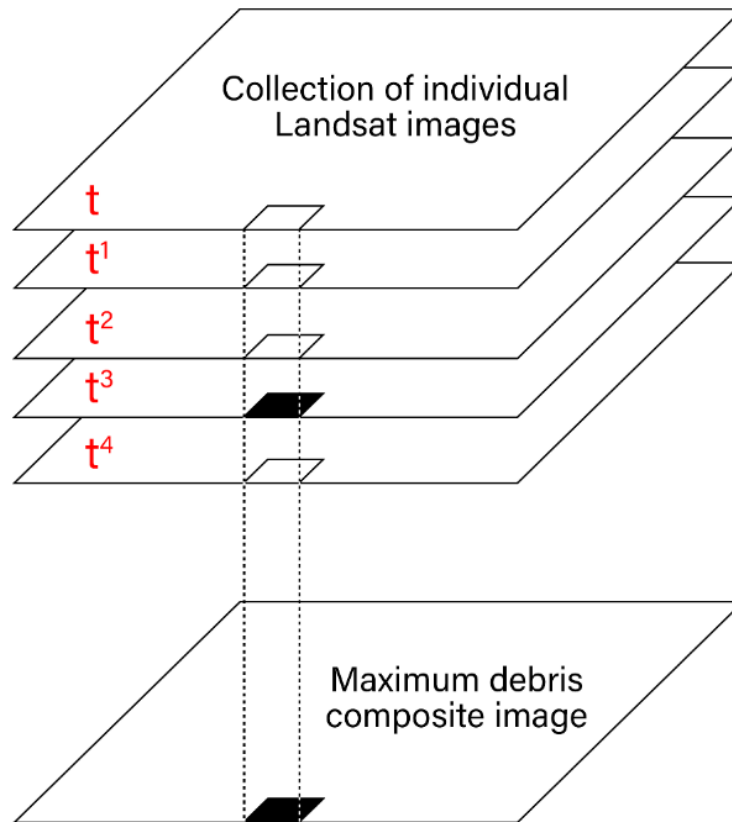
Figure 2: Reducer diagram - GEE stacks all images in the collection and undertakes pixel-wise analysis of debris cover, to create a mosaic of maximum debris cover extent. If just one pixel in the image stack is debris, then the corresponding pixel in the maximum debris mosaic will be debris. White pixels represent snow/ice, black pixels represent debris.

Earth **Surface**
Dynamics
Discussions
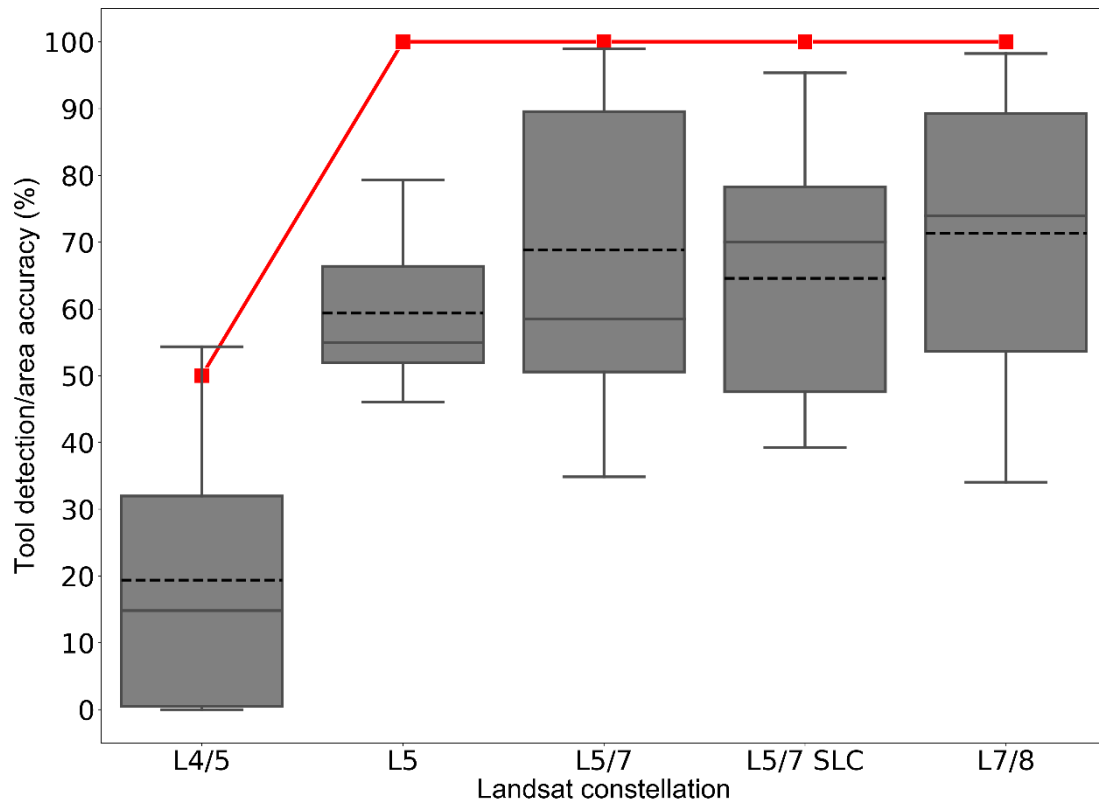
Figure 3: GERALDINE rock avalanche (RA) detection accuracy (red line) and RA area accuracy (boxplots) with different Landsat constellations over time. L4/5 (1984-1993) – 8 validation RAs, L5 (1993-1999) – 8 validation RAs, L5/7 (1999-2003) – 9 validation RAs, L5/7 SLC (Scan Line Corrector failure) (2003-2013) – 11 validation RAs, and L7/8 (2013-present) – 12 validation RAs. Dashed line represents mean, solid line median, box represents upper and lower quartiles, whiskers represents min and max area accuracies.
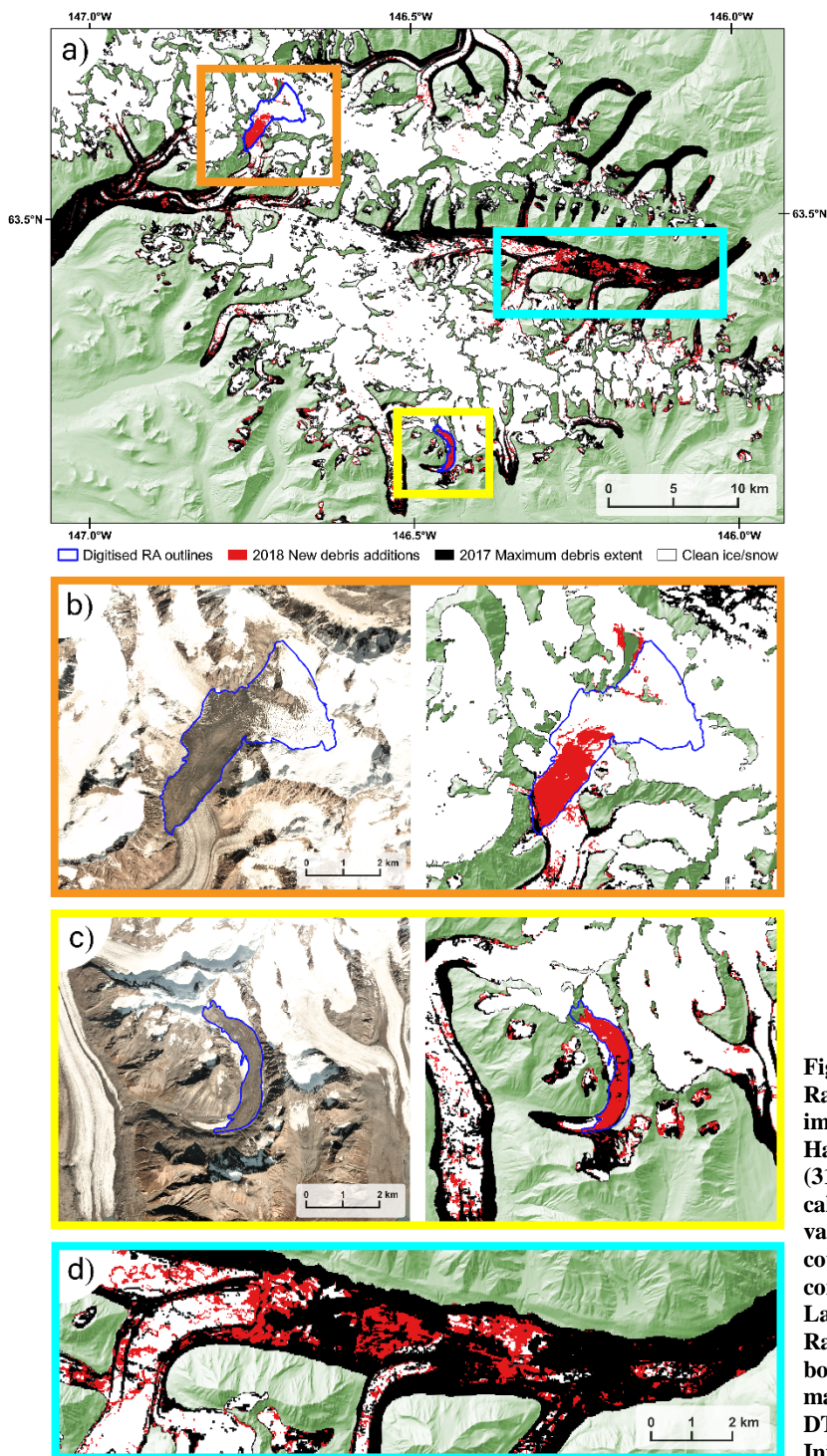
Figure 4: a) 2018 new debris additions in the Hayes Range, Alaska. RA outlines digitised using Landsat imagery and the GEEDiT tool (Lea, 2018). b) Mt Hayes RA image courtesy of Planet Labs, Inc. (31/07/2018) and corresponding tool detection extent calculated using Landsat imagery. c) RA on a small valley glacier East of Maclaren glacier, image courtesy of Planet Labs, Inc. (13/09/2018) and corresponding tool detection extent calculated using Landsat imagery. d) 2018 tool detection of Black Rapids glacier RA deposits. Orange, yellow and blue boxes signify areas of interest and correspond to magnified areas of b), c) and d), respectively. IFSAR DTM background from the Alaska Mapping Initiative (doi: 10.5066/P9C064CO)
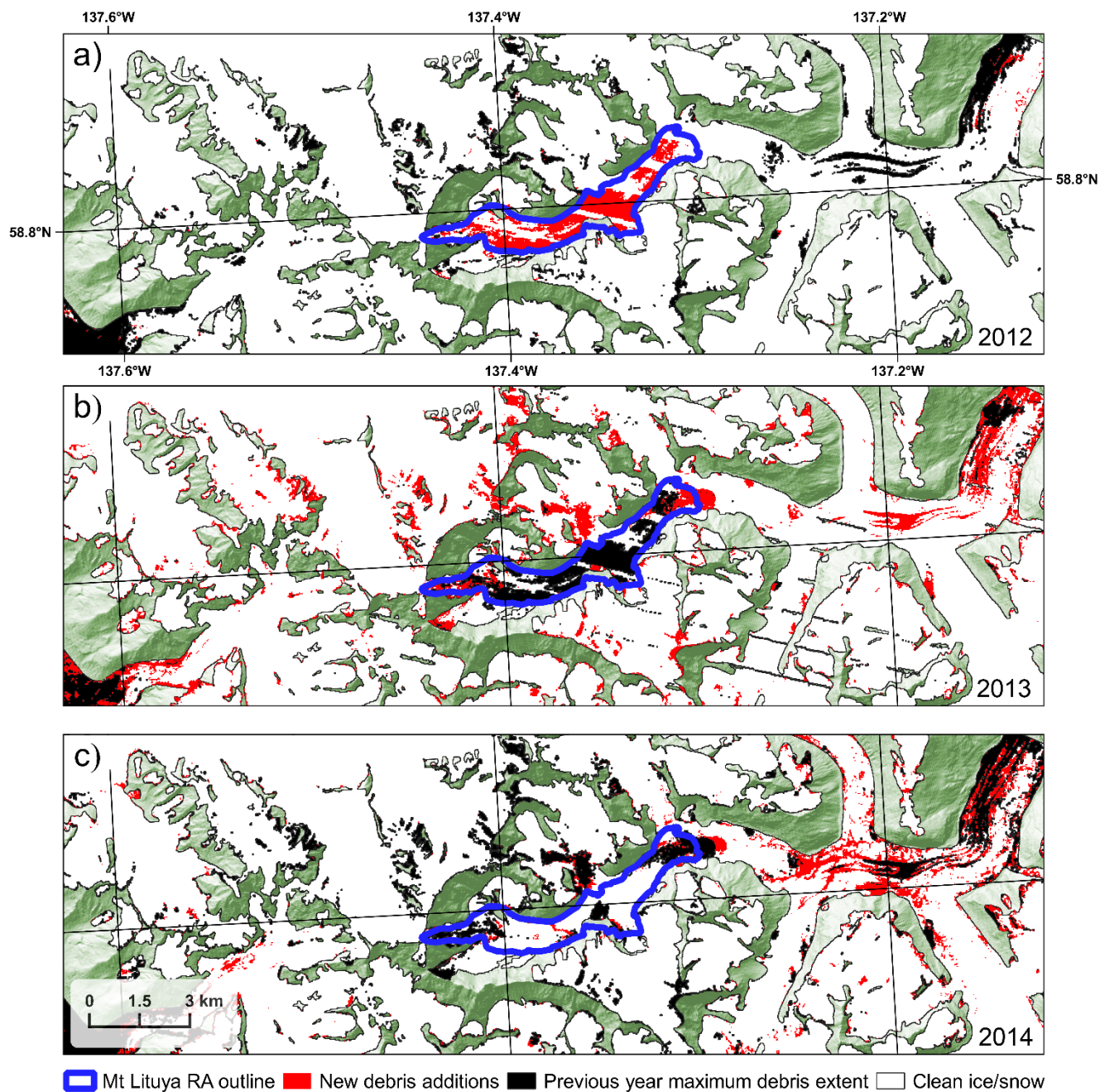
Figure 5: Deposition and behaviour of Lituya RA, John Hopkins Glacier Alaska (58°48'54.3''N, 137°17'40.9''W) detected by GERALDINE when run for a) 2012, b) 2013, and c) 2014. Landsat 7 scan line corrector issue visible in lower right section of 2013 image (B). IFSAR DTM background from the Alaska Mapping Initiative (doi: 10.5066/P9C064CO).